

Effect of Vibration and Noise Measuring Points Distribution on the Sensitivity of Pump Cavitation Diagnosis

Runze Zhou^{1,*} – Hui Chen^{2,3} – Liang Dong⁴ – Houlin Liu⁴ – Zeyu Chen¹ – Yuhang Zhang¹ – Zhiming Cheng¹

¹ Jiangsu University, Research Center of Fluid Machinery Engineering and Technology, China

² Science and Technology Laboratory on Liquid Rocket Engine, China

³ Xi'an Aerospace Propulsion Institute, China

⁴ Jiangsu University, National Research Center of Pumps, China

Cavitation is an essential factor in the deterioration of the hydraulic performance of centrifugal pumps. The study of cavitation fault diagnosis can help prevent or reduce the damage it causes. The vibration and noise analysis method can predict the incipient cavitation more accurately. In order to improve the accuracy of cavitation fault diagnosis, this paper studied the sensitivity of measuring points distribution for centrifugal pump cavitation diagnosis. The research object is a centrifugal pump with an inducer and splitter blades. Vibration acceleration sensors and hydrophones were used to collect structural vibration and liquid-borne noise signals at different positions of the pump unit. Root-mean-square (RMS) and fast Fourier transform (FFT) methods were used to construct spectrums of vibration and noise signals with different NPSHa and compare the sensitivity of different measuring points to the inception and development of cavitation. In addition, the SST $k-\omega$ turbulence model and Zwart cavitation model were used to study the cavitation volume distribution in the pump under different cavitation stages. By setting monitoring points at the impeller outlet, the frequency domain signal distribution of pressure pulsation was studied. The results show that the vibration measuring points at the inlet flange and pump axial position (increased by about 0.6 % at NPSHr) and liquid-borne noise measuring point at the inlet position (reduced by about 14 % at NPSHr) are more sensitive to the diagnosis of cavitation fault. Motor current is also the basis for judging the inception of cavitation. When severe cavitation occurs, the current drops sharply by approximately 12 %. Moreover, the pressure pulsation intensity at the inlet decreases by 66.3 % and by increases 13.9 % at the outlet, respectively, with a 3 % drop in head. As the cavitation intensifies, the dominant frequency of the pressure pulsation in the pump is partially shifted. The presented results indicate the distribution of measuring points with good sensitivity, providing a reference for improving the accuracy and efficiency of cavitation predictions for centrifugal pumps.

Keywords: cavitation diagnosis, centrifugal pump, vibration and noise, sensitivity of measuring points, spectral analysis

Highlights

- The spectral characteristics of centrifugal pump vibration and noise with the development of cavitation were revealed.
- The variations of pressure pulsation RMS and frequency domain with NPSHa were studied.
- The sensitivities of the cavitation diagnosis methods were verified, and the optimal measuring point layout scheme was proposed.
- The relationship between vapour volume evolution and noise frequency features was studied.

0 INTRODUCTION

Cavitation affects the operational stability and efficiency of the pump and is an essential indicator of pump performance. Generally, cavitation occurs when the absolute static pressure at the pump inlet is below the saturation vapor pressure, resulting in a disturbance and disruption of the energy exchange between the impeller and the liquid, and a significant reduction in the external characteristic curve. In severe cases, the liquid flow in the pump can be interrupted, causing the pump not to operate properly. The bubbles are transported to the high-pressure area and ruptured in a very short time, generating massive shock waves. The rupture of the bubbles causes severe damage to the impeller surface material in the form of pitting and erosion, resulting in the pump producing vibration

and noise [1]. It is not possible to suppress cavitation completely. Therefore, to ensure the reliability of pump operation, it is necessary to accurately detect the onset and development of cavitation, and control the operating conditions to prevent cavitation.

The development of cavitation is mainly divided into the inception, development, and degradation stages [2] to [5]. During the different stages of cavitation, there are variations in the quantities of pressure, flow rate and motor power. These features can be used to diagnose the severity of cavitation. The net positive suction head (*NPSH*) is commonly used in engineering to determine the operating conditions and suction performance. According to the ISO 3555 standard [6], the *NPSH* value for a 3 % drop in the total delivery head is defined as *NPSH*-required (*NPSH_r*), representing cavitation that has fully developed. When

*Corr. Author's Address: Research Center of Fluid Machinery Engineering and Technology, Jiangsu University, Zhenjiang, China, 798917967@qq.com

the cavitation occurs, it causes a change in pump load torque. The electric signal in the motor can evaluate the impeller torque, which can detect the beginning of cavitation. Meanwhile, cavitation can be predicted by measuring the line voltage and phase current on the power transformer [7] and [8]. The normalized amplitude at the third-order rotational speed obtained by measuring the instantaneous angular velocity of the pump and the order spectrum analysis can also be used for characteristic monitoring [9]. Vibration and noise are generated due to the continuous rupture of the bubbles in the high-pressure region accompanied by strong water shock during vapourization inside the pump. There is a discrete frequency or broadband peak in the audible noise spectrum, which is closely related to the development of cavitation. The discrete frequencies are consistent with the $NPSH_r$, and both can correspond to a 3 % drop in the total delivery head. The characteristic discrete frequency tones closely associated with cavitation are the resonance caused by structural vibrations or the rupture of bubbles on the inner wall surface of the pump, so the discrete frequency tones can detect the intensity of cavitation. The measurement methods are mainly divided into three types: sound pressure level in air, underwater acoustics and structural vibration [10] to [12]. Černetič [13] and Černetič and Čudina [14] evaluated the uncertainty of cavitation prediction for vibration and noise signals from centrifugal pumps in broad frequency range and at discrete frequencies, verifying that vibration and noise in the audible frequency range are capable of predicting and diagnosing cavitation. Chini et al. [15] analysed the noise spectrum of centrifugal pumps to find the feature of cavitation initiation and found that sound pressure levels at some frequencies can detect the inception of cavitation and quantify the severity of cavitation. Wang et al. [16] found that as cavitation intensifies, the vibration acceleration and noise stabilize at first and then increase apparently, which can determine the $NPSH$ -inception of the pump. Zhang et al. [17] found that the cavitation critical point inferred from the vibration level is higher than the $NPSH_r$ when the head drops by 3 %, indicating the actual cavitation time is earlier than that reflected by the head curve. Dong et al. [18] found that with the decrease of $NPSH$, the total sound pressure level of liquid-borne noise first increase and then decreases, and the sound pressure level of liquid-borne noise in the 2 kHz to 3 kHz frequency range can better predict the initiation of cavitation, with a threshold value of 1 %. Al-Obaidi [19] to [22] used time-domain analysis (TDA) and fast Fourier transform (FFT) techniques for frequency

domain analysis (FDA) based on vibration and acoustic analysis methods. The ability of the different methods to diagnose pump cavitation under different operating conditions was compared and evaluated, proposing that peak and peak-to-peak values are more sensitive to cavitation detection in pumps than the RMS and variance feature. Mousmoulis et al. [23] concluded that the impeller's geometric parameters affect the development of cavitation, and that acoustic and vibration measurements can effectively predict cavitation.

Many researchers have asserted that the signal features of vibration, noise, and pressure pulsation can effectively predict the initiation and development of pump cavitation, and proposed signal processing and analysis methods to detect cavitation. However, there is a lack of studies on the sensitivity of measuring point distribution for cavitation prediction. In practice, the characteristics of the vibration signal at different positions are dissimilar. And the liquid-borne noise and pressure pulsation characteristics of the inlet and outlet have different sensitivities to cavitation prediction. Therefore, the location of the measuring points has a crucial influence on the accuracy of cavitation fault diagnosis. To improve the prediction of cavitation and reduce the damage to the pump, it is necessary to research the effect of measuring point distribution on cavitation fault diagnosis.

In the actual operation of the pump, the flow rate is reduced due to the influence of cavitation. In some special applications, there are high demands on the stability of the pump flow rate, for example, fuel pumps for the liquid rocket engine. The cavitation test is usually carried out by keeping the flow rate at a constant value [24], which can intuitively evaluate the cavitation performance of the centrifugal pump. However, it cannot restore the actual situation properly. This paper took a small flow rate and high head centrifugal pump with an inducer and splitter blades as the research object. The valve opening was constant during the cavitation test so that the flow rate varied continuously with the development of cavitation. In addition, hydrophones and high-frequency pressure sensors were installed at the inlet and outlet, and eight vibration sensors were installed at the inlet and outlet flanges, the pump axial and radial, the pump foot, and the bearing housing. The signal characteristics at different locations under different cavitation conditions were measured. The sensitivity of different measuring points was analysed to obtain the optimum method for detecting the onset and development of cavitation in centrifugal pumps and improving the accuracy of cavitation fault diagnosis in centrifugal pumps.

1 TEST AND SIMULATION METHODS

1.1 Research Object

The test bench comprises a vibration and noise high-frequency signal test system, an external characteristic test system and a data acquisition system. Fig. 1a shows that the test equipment includes a cavitation tank, a vacuum pump, pipelines, valves, an electromagnetic flowmeter, test pumps, motors, pressure transmitters, hydrophones, vibration acceleration sensors, and pressure pulsation sensors. The pressure transmitters are located at two times the pipe diameter of the pump inlet and outlet flange. The hydrophones and pressure pulsation sensors are installed eight times the pipe diameter. Moreover, the vibration acceleration sensors are installed in eight positions: inlet flange vertical and horizontal, outlet flange vertical and axial, pump body radial, axial and foot, and the bearing house, as shown in Fig. 1b.

A small flow rate and high head centrifugal pump with a specific speed of 25 was used as the research object, and the equation for the specific speed is as follows [1]:

$$n_s = \frac{3.65n\sqrt{Q}}{H^{3/4}}. \quad (1)$$

The design parameters of the pump are flow rate $Q_d=5 \text{ m}^3/\text{h}$, head $H_d=39 \text{ m}$, and rotational speed $n=2900 \text{ r/min}$. The centrifugal pump impeller has four main blades and four splitter blades, the diameter of the impeller $D_j=160 \text{ mm}$, the outlet width of the impeller $b_2=6.5 \text{ mm}$, and the blade wrap angle $\varphi=80^\circ$. The inducer has a tapered hub with equal pitch double blades. The axial length of the hub is $h_h=40 \text{ mm}$, the axial length of the rim $h_y=30 \text{ mm}$, and the inlet sweep angle $\theta_1=140^\circ$. The structure of the test pump is shown in Fig. 2.

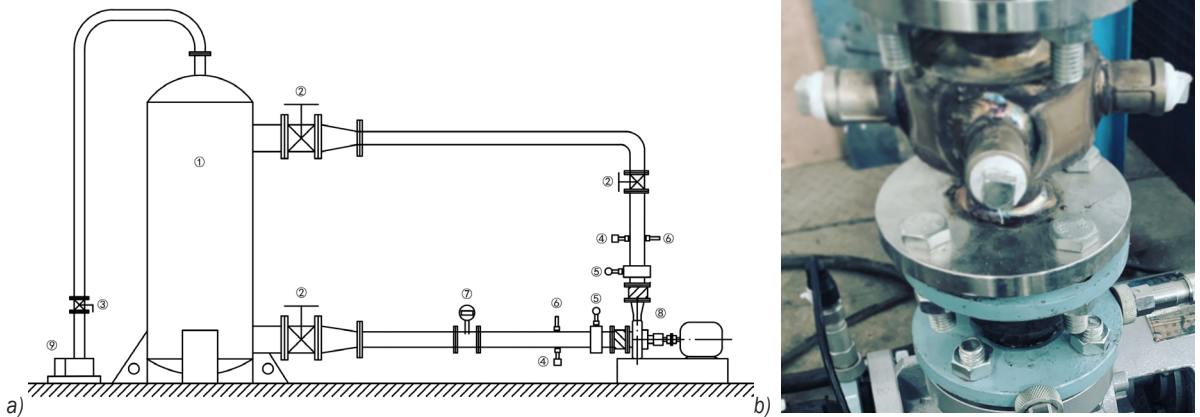


Fig. 1. Centrifugal pump cavitation test bench; a) test bench (1. cavitation tank, 2. gate valve, 3. ball valve, 4. pressure pulsation sensor, 5. pressure transmitter, 6. hydrophone, 7. electromagnetic flowmeters, 8. pump set, 9. vacuum pump), and b) vibration measuring points

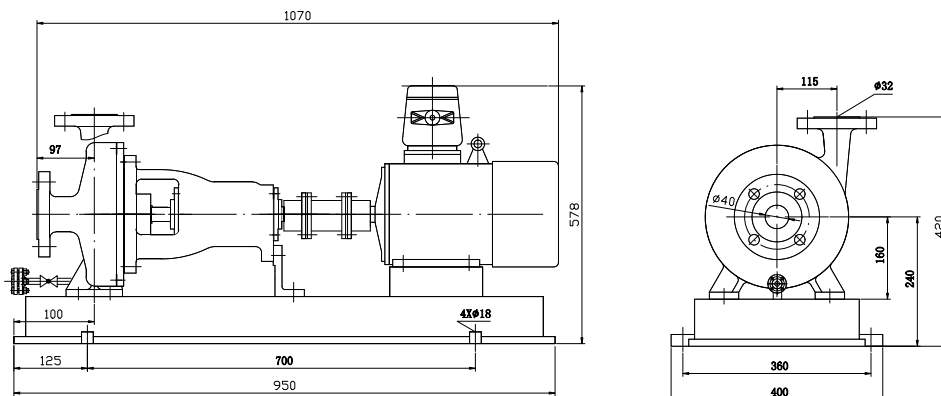


Fig. 2. Two-dimensional structure of test pump

1.2 Test Method

The centrifugal pump cavitation tests are usually carried out at a constant flow rate [1], which means that the outlet valve is controlled to keep the flow rate unchanged. The pressure at the inlet is reduced by a vacuum pump, causing the pump to cavitate. This method can effectively obtain the cavitation performance curve of the pump at a fixed flow rate. However, in many practical applications, it is impossible to adjust the valve in time to keep the flow rate constant. The flow rate decreases with the intensification of cavitation and even breaks down. For example, the heavy drop in flow rate caused by cavitation can result in the turbopump being unable to supply oxidizer to the liquid rocket engine in time, leading to severe operational failure of the rocket. Very few cavitation tests with a fixed valve have been carried out, specifically with the flow rate changes as cavitation. Therefore, this paper used this method to conduct cavitation tests and measured pressure pulsation, vibration and noise signals.

The vibration and noise signal under cavitation is significantly different from other mechanical faults in terms of spectral distribution. The broadband character of cavitation has an effect not only on low-frequency signals but also on the higher frequency bands [25]. According to the Nyquist-Shannon sampling theorem, the sampling frequency is more than twice the highest frequency in the signal, so that the information in the original signal is not lost from the acquired digital signal. In order to make the acquired signal reflect the trend in the high-frequency band and ensure the accuracy in the low-frequency band, a sampling frequency of 10 kHz is used to acquire the signal, considering the sensors' operating range and each sampling time is 3 s. And the test steps are as follows.

1. Adjust the pump motor speed to 2900 rpm by frequency converter.
2. Control the outlet valve to stabilise the initial flow rate at 5 m³/h.
3. Turn on the vacuum pump and reduce the inlet pressure of the centrifugal pump.
4. Obtain signals for flow rate, pressure pulsation, liquid load noise and structural vibration at different *NPSHa*.

The data were processed and analysed using MATLAB software. The vibration and noise signals are processed as follows:

(1) Vibration acceleration levels

The intensity of vibration (i.e. the energy of vibration), is commonly expressed by physical

quantities such as velocity, acceleration and displacement. In contrast, acceleration can better reflect the impact of vibration on the structure. Therefore, the RMS value of acceleration is generally used to express the intensity of the vibration. In practice, the vibration is compound: not a single frequency vibration but superimposed vibrations of multiple frequencies. For evaluating vibration energy, one of the commonly used evaluation indicators is vibration acceleration level. The vibration acceleration level *VAL* is defined as [26]:

$$VAL = 20 \lg(a_r / a_0), \quad (2)$$

where a_r is the RMS of acceleration, and a_0 is the reference acceleration, generally $a_0 = 10^{-6} \text{ m/s}^2$. The unit of vibration acceleration level is decibel, [dB]. And the RMS of vibration acceleration a_r defined as follows [26]:

$$a_r = \sqrt{\frac{1}{T} \int_0^T a_i^2(t) dt}, \quad (3)$$

where $a_i(t)$ is the acceleration at some point, and T is the total number of samples.

(2) Sound pressure level

The hydrophone is affected by the hydroacoustic sound pressure P in the sound field, which generates an open-circuit voltage U . The open-circuit voltage U is proportional to the sound pressure P . Therefore, the hydrophone sensitivity M can be obtained as [27]:

$$M = U / P, \quad (4)$$

where U is usually defined as the open-circuit voltage generated when the hydrophone is subjected to 1 Pa liquid-borne sound pressure in the sound field.

The sensitivity is compared with the reference value and then taken logarithmically to obtain its corresponding decibel value. In hydroacoustics, 1 μPa is usually used as the sensitivity reference. The output voltage signal of the hydrophone is processed by the FFT method to obtain the voltage spectrum and logarithmically transform the voltage spectrum to obtain the voltage decibel [27]:

$$U_{dB}(f) = 10 \lg(U_{FFT}(f)), \quad (5)$$

where $U_{FFT}(f)$ is the amplitude of the hydrophone's voltage spectrum at some frequency.

The sound pressure level of the liquid-borne noise at this frequency is obtained by subtracting the voltage decibel from the sensitivity of the hydrophone [27]:

$$SPL = U_{dB}(f) - M(f). \quad (6)$$

Similar to the total vibration level calculation, the total sound pressure level of liquid-borne noise is calculated as follows [27]:

$$SPL_t = 20 \lg(p / p_{ref}), \quad (7)$$

where p is the RMS of sound pressure, and p_{ref} is the reference value of underwater sound pressure, 1 μ Pa.

1.3 Numerical Simulation Method

Creo 5.0 was used to build the 3D model of the pump. The entire model was divided into five parts: the inlet pipe, the inducer, the impeller, the volute and the outlet pipe. ANSYS-ICEM 17.0 was adopted to generate tetrahedral grids, as shown in Fig. 3. To meet the requirements of numerical simulation on grid quality, the grids around the volute tongue and blades are improved and smoothed. The average y^+ of the grid model is less than 80. Five sets of grids with different cell numbers were generated to verify the grid independence, as listed in Table 1. The judgment basis was that head error of less than 1 % and the time cost of the calculation is as short as possible. The second grid set is closer to the actual parameters in terms of head and has fewer cells than the other sets. Therefore, this paper used this grid for numerical simulation.

Fig. 4 compares the external characteristic results of the numerical simulation with the test. The trend

of the numerical simulation and the test result is the same. As the flow rate increases, the head of the centrifugal pump tends to decrease, and the efficiency increase significantly. The head and efficiency at each operating point obtained by the numerical simulation are consistent with the test results, and the maximum error does not exceed 3 %. Therefore, the numerical simulation results have good accuracy.

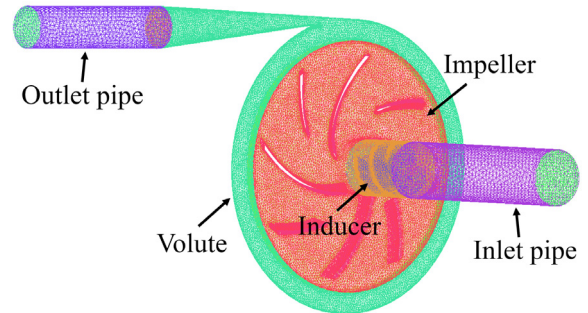


Fig. 3. Grid model

The ANSYS-CFX17.0 software was applied to numerically simulate the cavitation of a centrifugal pump at different inlet pressures. The pump's inlet and outlet boundary conditions were set according to the inlet pressure and the flow rate results obtained by the test at different $NPSHa$. The evolutions of the internal flow field and vapour volume under different cavitation stages were obtained through numerical

Table 1. Grid independence verification

Program	Inlet and outlet section	Volute	Inducer	Impeller	Total	Head [m]	Error [%]
1			1.18×10^6	1.53×10^6	4.11×10^6	39.18	0.46
2			9.22×10^5	1.04×10^6	3.37×10^6	39.14	0.35
3	6.42×10^5	7.61×10^5	7.81×10^5	9.43×10^5	3.13×10^6	39.31	0.79
4			6.21×10^5	8.21×10^5	2.85×10^6	40.26	3.23
5			5.35×10^5	7.43×10^5	2.68×10^6	40.32	3.49

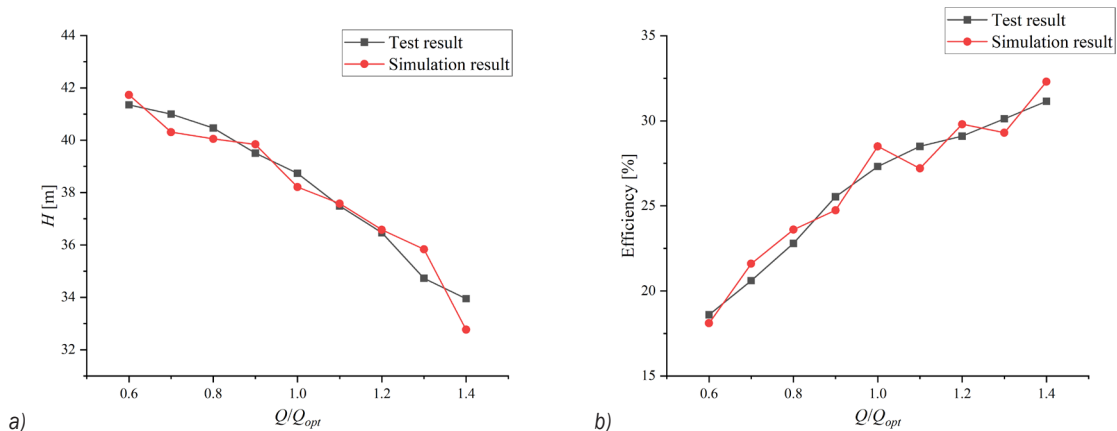


Fig. 4. Comparison between simulation results and test results, a) Q-H curve, and b) Q-Efficiency curve

simulation. The turbulence model uses the shear stress transport $k-\omega$ (SST $k-\omega$). This model is widely used in rotating machinery [28]. The SST $k-\omega$ can better calculate the adverse pressure gradient and separation flow. It predicts the pump's performance more accurately [5]. The rotor-stator interfaces use the transient rotor-stator. The pitch change is specified pitch angles with a value of 360° , and the interface between the impeller and the inducer is relatively stationary. The grid connection between the interfaces is set as the general grid interface (GGI). The fixed wall adopts no-slip, and the rotating walls on the impeller and inducer are moving walls. The advection scheme adopts the high resolution, and the transient scheme adopts the second-order backward Euler. The maximum number of inner iteration loops is set to 20. The residual accuracy was $10e^{-4}$. The rotational speed is 2900 rpm. The time step is the time taken for each 2° rotation of the impeller, i.e. 0.00011494 s. The total time step is the time taken for five cycles of the impeller. The steady-state results are taken as the initial values for the unsteady-state calculations.

The fluid medium is water at 25°C . The gas medium is set to water vapour at 25°C , the Saturation Pressure of the fluid is 3169 Pa, the reference pressure is 0 Pa, the volume fraction of the inlet vapour is set to 0, and the volume fraction of the liquid is set to 1. The Zwart cavitation model is used. The net positive suction head available ($NPSHa$) of the pump is calculated as [1]:

$$NPSHa = \frac{P_s - P_v}{\rho g} + \frac{v_s^2}{2g}, \quad (8)$$

where P_s is the pump inlet pressure; P_v is the saturated vapour pressure of the fluid at operating temperature; v_s is the flow rate at the pump inlet.

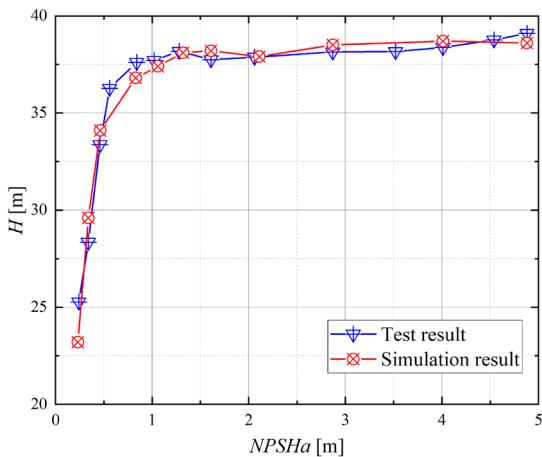


Fig. 5. Comparison of cavitation performance curves

Fig. 5 shows the cavitation performance curves obtained from the tests and numerical simulations. The trends in the cavitation performance curves are generally consistent, although there are some errors between the simulation and test results. The inception points of cavitation in test and simulation are almost the same. The $NPSHr$ measured by the test is 1.03 m, while the simulation result is 1.06 m, with an error of about 3 %. When the head drops by 10 %, the $NPSHa$ values of both are also very close. Therefore, the simulation results can more accurately reflect the evolution of cavitation.

2 ANALYSIS OF CAVITATION PREDICTION METHODS

2.1 External Characteristics

Fig. 6 shows the flow rate and head variation curves for different $NPSHa$ obtained from cavitation test with fixed valve. A slight drop in the head occurs as the $NPSHa$ decreases from 5 m to 2 m. At $NPSHa = 3.83$ m, the head drops by approximately 1 %. There is some fluctuation in flow rate but no significant drop. When $NPSHa$ reduces from 2 m to 1.5 m, the head and flow rate both decrease first and then rise. With the decrease of $NPSHa$ (1.5 m to 0.5 m), cavitation in the pump begins to develop continuously, and the head and flow rate decrease again. When $NPSHa = 1.02$ m, the head drops by 3 %, which is the net positive suction head required ($NPSHr$), meaning that full cavitation has occurred at this time [6]. Cavitation continues to intensify after the $NPSHa$ falls below 0.5 m. The flow rate and head drop drastically, and the pump has a significant loss of hydraulic performance.

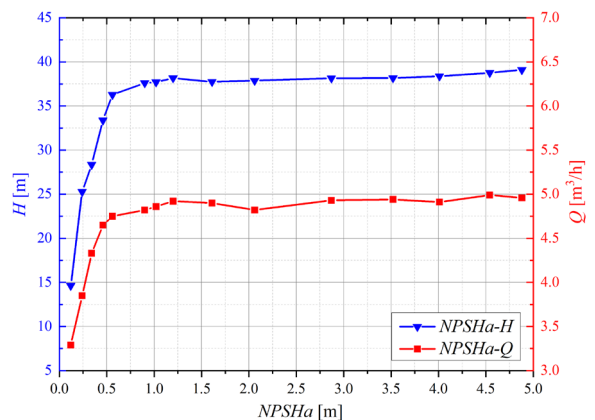


Fig. 6. Variation of head and flow rate with $NPSHa$

At the same time, with the decrease of inlet pressure, the current affected by cavitation also changes obviously, and it has regularity. As shown in

Fig. 7, during the process of $NPSHa$ falling from 5 m to 2 m, the overall current shows a downward trend. When $NPSHa = 2$ m, the current decreases by 2 %, then there is a rebound. After the $NPSHa$ drops below 1.2 m, the current decreases continuously. And when $NPSHa$ is less than 0.5 m, the current drops sharply, by about 12 %. Therefore, consistent with the method proposed in [8], the onset of pump cavitation can be detected by the motor phase currents.

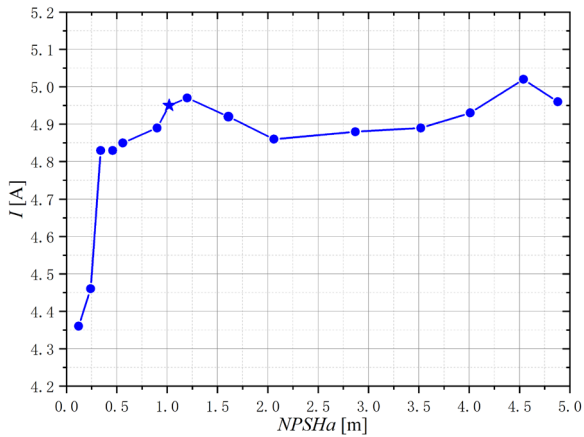


Fig. 7. Variation of motor current with $NPSHa$

2.2 Structural Vibration Signals

The variation curves of vibration acceleration levels for each measuring point at different $NPSHa$ as shown in Fig. 8. The vibration acceleration level at each measuring point fluctuates slightly during the non-cavitation stage but remains low. As the $NPSHa$ reach the onset of cavitation, the vibration acceleration levels increase significantly, and as the degree of cavitation increases, the vibration acceleration levels

rise rapidly after reaching the peak, and then decline. The results are close to the trend of the vibration acceleration on the pump casing in [10], and the rise rate of the vibration acceleration level at $NPSHr$ is also similar. Comparing the eight measuring points, the vibration acceleration level at the Bearing house is the highest. However, the overall curve change rate is relatively small, while the vibration acceleration levels of the other measuring points increase significantly during the cavitation development phase. The point marked by the star symbol in the figure is the head drop of 3 %, that is, the vibration acceleration level of each monitoring point at the $NPSHr$. The vibration acceleration level at the outlet flange is higher than that of the inlet flange. However, the amplitude change at the inlet flange is more pronounced, rising by approximately 0.6 % at $NPSHr$. In the non-cavitation stage, the vibration acceleration of the pump radially is larger than the pump axially. With the intensification of cavitation, the vibration acceleration level at the pump axial significantly exceeds that at the pump radial, and increases by about 0.5 % at $NPSHr$.

Fig. 9 shows the vibration acceleration levels spectrum with cavitation development at different measuring points. The trend of each measuring point shows that as the cavitation continues to increase, there is an evident broadband characteristic. The inlet flange horizontal and vertical measuring points have a strong signal distribution in all frequency bands during the non-cavitation phase, but the overall distribution is dispersed. After the onset of cavitation, the vibration signal in the 500 Hz to 4500 Hz frequency band enhances significantly. The outlet flange measuring point is mainly concentrated below 1000 Hz and in the band of 2000 Hz to 3500 Hz. With the $NPSHa$ decreasing, the signal change in the range

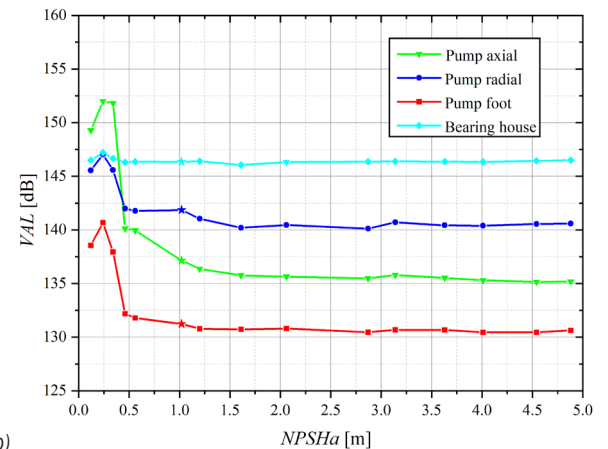
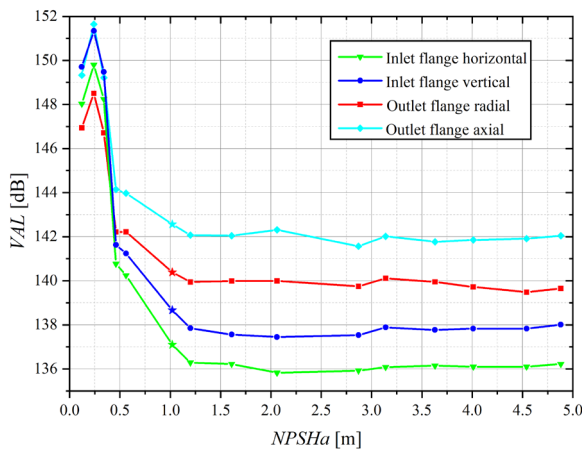


Fig. 8. Trends of the total VAL of each measuring point with $NPSHa$; a) inlet and outlet measuring points, and b) pump body measuring points

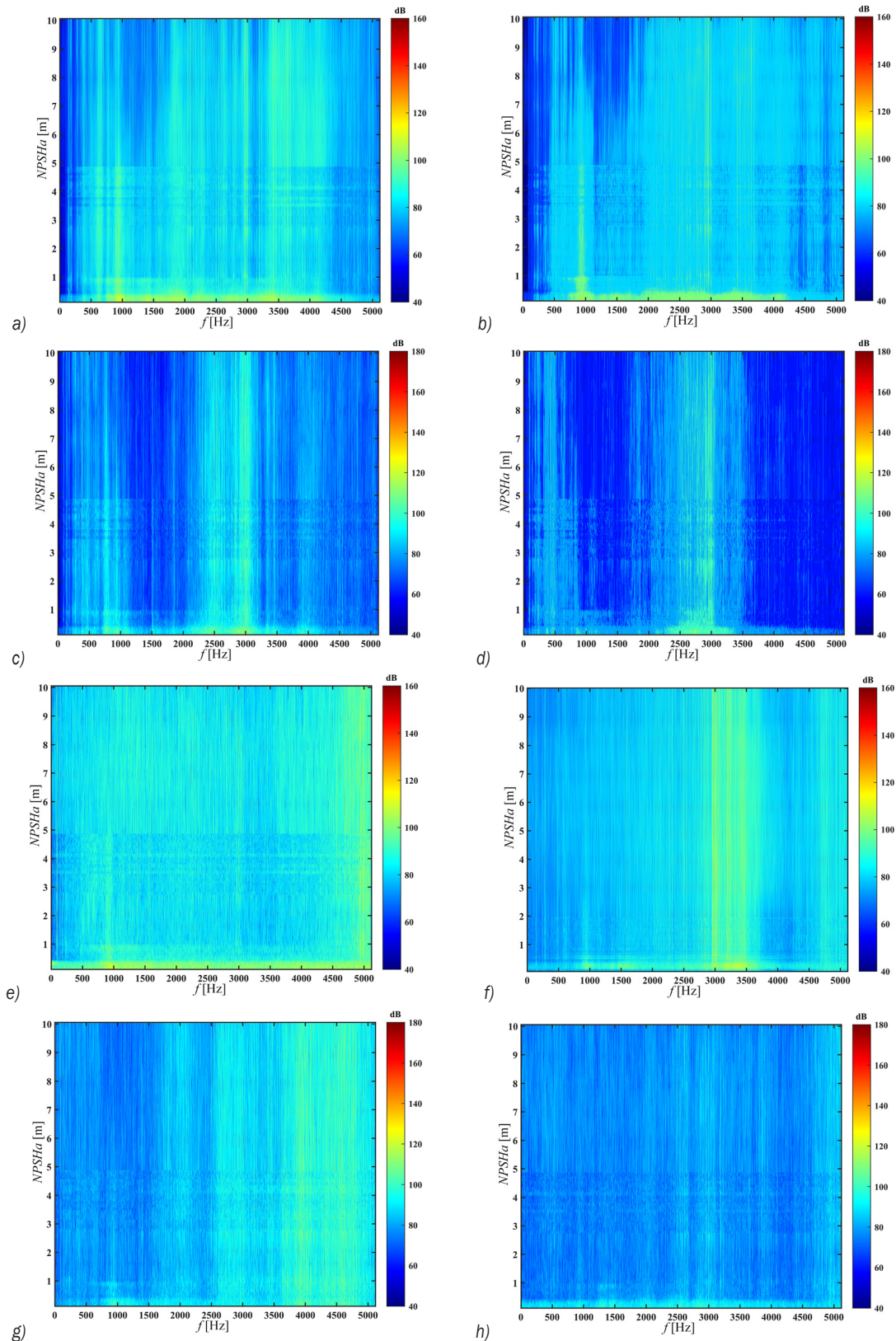


Fig. 9. VAL frequency characteristics of each measuring point with NPSHa; a) inlet flange horizontal, b) inlet flange vertical, c) outlet flange radial, d) outlet flange axial, e) pump axial, f) pump radial, g) pump foot, and h) bearing house

of 2000 Hz to 3500 Hz is more obvious. In contrast, the inlet measuring point is more sensitive to the onset of cavitation. The pump body axial measuring point shows a strong vibration signal appears in all frequency bands. The spectrum distribution at the pump body radial is also broader, and the vibration acceleration level signal in 3000 Hz to 3500 Hz is intense. However, with the development of cavitation, the variation of the vibration acceleration level signal in the whole frequency range is not as pronounced as that of pump body axial. The bearing house measuring point has a relatively strong amplitude in the high-frequency band, while the overall vibration acceleration level of the pump foot is small, and the signal distribution is relatively sparse. Both spectral variations are not sufficiently apparent and less sensitive to the onset of cavitation.

2.3 Liquid-borne Noise Signals

With the decrease of inlet pressure, $NPSHa$ continuously decreases, and the frequency domain

of the peak signal of the inlet and outlet liquid-borne noise gradually shrinks, as shown in Fig. 10. As the cavitation effect intensifies, the signal above 120 dB inlet almost disappears. The sound pressure level in 1000 Hz to 5000 Hz at the outlet drops below 100 dB. The length of the vapour attached to the blade's working surface increases, and there are large oscillations in the tail of the cavitation. It causes the bubbles to fall off, and the unstable cavitation intensifies, thus leading to broad frequency pulsations in the low-frequency band of the liquid-borne noise. Moreover, because the cavitation in part of the flow channel blocks the entry of the main flow, the number of effective flow channels is reduced, thereby changing the frequency distribution of the liquid-borne noise. Although there is also a more pronounced change in the outlet liquid-borne noise signal, the variation is insignificant compared to the inlet. Fig. 11 shows that with the decrease of the $NPSHa$, the inlet liquid-borne noise presents a continuous decreasing trend, which is similar to the trend in [10]. However, the sound pressure level of the liquid-borne noise at

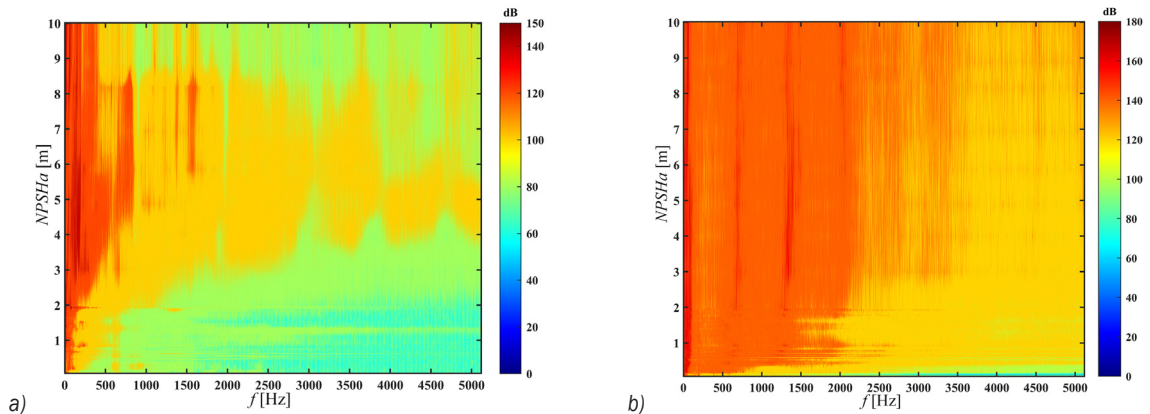


Fig. 10. Liquid-borne noise frequency characteristics; a) at the inlet, and b) at he outlet with $NPSHa$

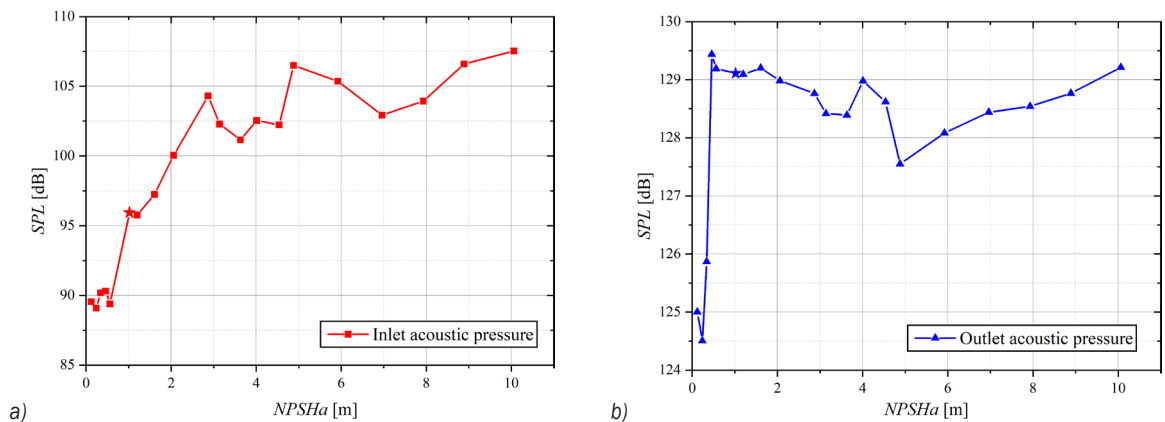


Fig. 11. Trends of a) inlet and b) outlet liquid-borne noise SPL with $NPSHa$

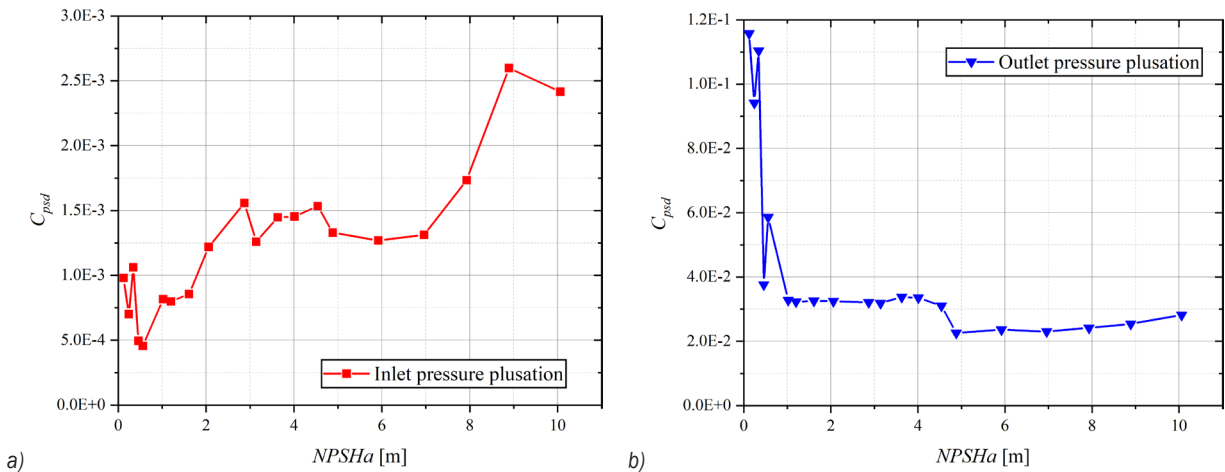


Fig. 12. Trends of a) inlet and b) outlet pressure pulsation PSD with $NPSHa$

the outlet first decreased, then increased, and finally decreased rapidly. At the net positive suction head required point, the inlet liquid-borne noise decreases by approximately 14 %, while the outlet liquid-borne noise decreases by approximately 1 %. The comparison shows that the inlet liquid-borne noise measuring point is more sensitive to the outlet.

2.4 Pressure Pulsation Signals

The power spectral density (PSD) method was used to process the pressure pulsation signal to determine the intensity of the pressure pulsation. Fig. 12 shows the pressure pulsation intensity coefficient as the $NPSHa$ decreases. It can be found that the inlet pressure pulsation shows a decreasing trend with the reduction of the $NPSHa$, while the outlet pressure pulsation is maintained first and then rapidly rising trend. When the head drops by 3 %, the inlet pulsation intensity decreases by 66.3 %, while the outlet pulsation intensity increases by 13.9 %. The inlet pulsation intensity shows an overall decreasing trend as the $NPSHa$ decreases. Although there are some fluctuations, it can better reflect the pressure pulsation intensity change with the development of cavitation. The outlet pressure pulsation does not change significantly before the onset of cavitation. When it is close to complete cavitation, the sudden rise occurs, and the rate of change is not as apparent as the inlet measuring point. Therefore, relative to the measuring point at the outlet position, the pressure pulsation measuring point at the inlet can better predict the inception and development of cavitation.

3 ANALYSIS OF NUMERICAL SIMULATION RESULTS

3.1 Vapour Volume Evolution

Fig. 13 shows the evolution in the volume fraction distribution of vapour under different $NPSHa$. As the $NPSHa$ decreases, the vapour volume in the impeller continues to extend from the blade inlet to the outlet. The development of vapor volume presented in the results is consistent with [4]. When the $NPSHa$ is 1.61m, it is the inception of cavitation. A lower level of vapour has appeared on the suction surface of the blade inlet, but there is no significant change in head and flow rate. When the $NPSHa$ is 1.34 m, the vapour volume area expands. At this time, the head does not decrease but instead increases slightly, which is due to the bubbles generated on the blade surface, which improve the flow state in the pump. When approaching the $NPSHr$, the vapour area begins to diffuse towards the blade working surface, and the flow rate and head drop by approximately 2.8 % and 3 %, respectively. At $NPSHa$ is 0.83, the vapour area spreads to the root of the splitter blade, occupying about one half of the flow channel, and the head drops by more than 5 %. While the flow rate drops slightly lags behind the head, dropping by about 3 %. As $NPSHa$ continues to decline, the vapour area occupies the entire flow channel of the impeller and flows into the diffusion section of the volute, blocking the flow channel. The flow rate and head drop by 27 % and 13.4 %, the pump's performance is seriously affected.

3.2 Pressure Pulsation Analysis

To investigate the characteristic changes of the pressure pulsation signal in the pump under different

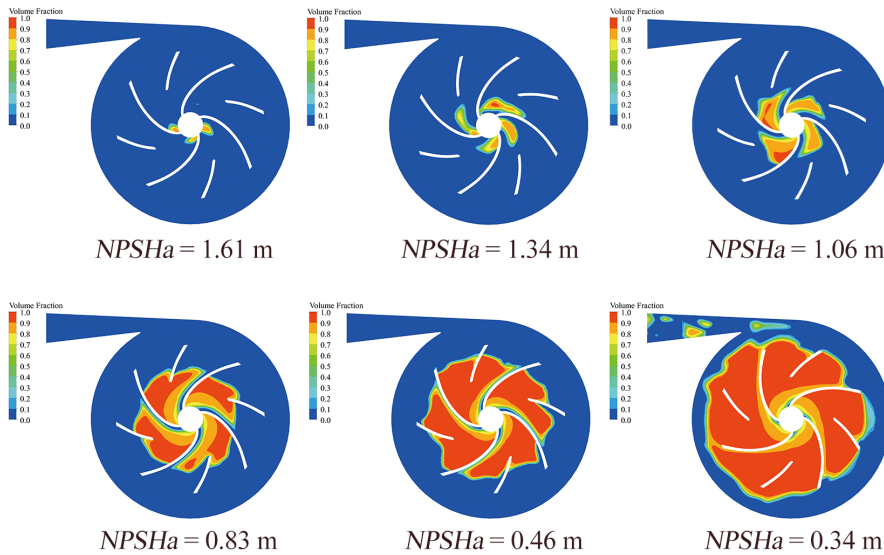


Fig. 13. Volume fraction distribution of vapor under different NPSHa

NPSHa, eight pressure pulsation monitoring points were set up at the interface between the impeller and the volute, and each monitoring point is separated by 45°, as shown in Fig. 14. The stable results of the last three cycles are extracted from the unsteady calculation. The fast Fourier transform (FFT) algorithm was used to calculate the discrete Fourier transform (DFT) of the pressure pulsation time-domain signal at different cavitation stages at each measuring point. The frequency-domain results are shown in Fig. 15.

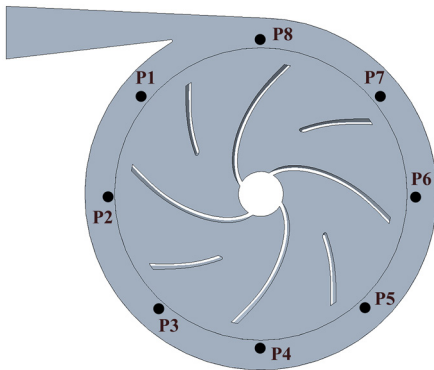


Fig. 14. Pressure pulsation measuring points

The impeller rotational speed is $n = 2900$ rpm, so the shaft frequency $f_r = 48.3$ Hz, the main blade passing frequency $f_{MBPF} = 193.3$ Hz, and the total blade passing frequency $f_{BPF} = 386.7$ Hz. In the non-cavitation phase, the main frequency of the pressure pulsation at the monitoring points P2 to P4 and P8 is the total blade passing frequency f_{BPF} of the impeller,

which is eight times the shaft frequency. The main frequency of P5 to P7 is the main blade passing frequency f_{MBPF} , (i.e., four times the axis frequency). When cavitation causes a 3 % drop in head, the main frequency is at the main blade passing frequency f_{MBPF} at all six monitoring points except for P3 and P7, where the main frequency is at the f_{BPF} . When the head drops by 5 %, the main frequency at P1 appears at two times the shaft frequency. The main frequency P3 is at the main blade passing frequency f_{MBPF} . For other monitoring points, the main frequency is at the total blade passing frequency f_{BPF} . When the head drops sharply by 30 %, the main frequency of some monitoring points shift. Except for P4, P5, and P6 at the f_{BPF} , the main frequencies appear at the 1/3 and 2/3 shaft frequency. As cavitation develops and the amplitude of the pressure pulsation signal increases, the interference at harmonic frequencies becomes severe. The main frequency of some monitoring points also has some changes.

4 CONCLUSIONS

This paper studied the influence of measuring point distribution for pump cavitation diagnosis. The liquid-borne noise, vibration acceleration and pressure pulsation at different positions of the pump units were measured through the fixed valve test. The RMS was used to process the signal data of each cavitation condition, which can better reflect the sensitivity of monitoring points to cavitation than the data analysis at the characteristic frequency in [10] and [13]. The sensitivities of different measuring points to predict

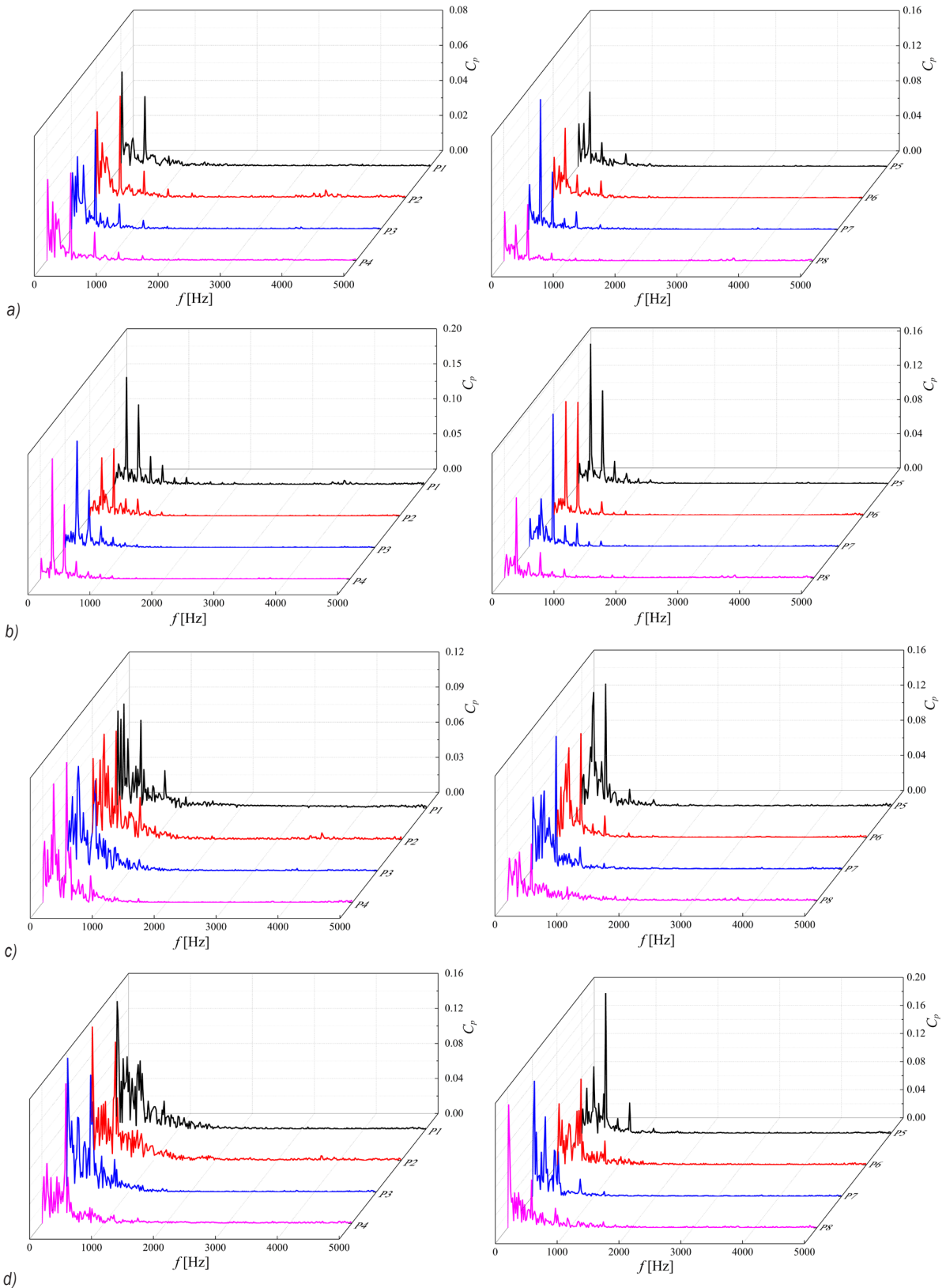


Fig. 15. Pressure pulsation frequency under different cavitation conditions;
 a) none-cavitation, b) 3 % drop in head, c) 5 % drop in head, d) 27 % drop in head

cavitation were compared. Furthermore, the SST $k-\omega$ turbulence model and Zwart cavitation model were used to numerically simulate the evolution of the vapour's volume distribution and pressure pulsation characteristics inside the pump.

With the development of cavitation, the flow rate decreases more slowly than the head. When the head drops by 3 %, the flow rate reduces by about 2.8 %. The motor current also shows a certain decrease, which can be used to predict the onset of cavitation and agrees with the findings [8]. When $NPSH_a$ is less than 0.5 m, the current drops sharply, about 12 %. The vibration acceleration level of each measuring point increases significantly. The measuring points of the inlet flange and the pump body axial are more sensitive to predicting cavitation, and both decreased by 0.6 %.

The frequency band of the liquid-borne noise peak shrinks significantly. At the $NPSH_r$ operating point, the sound pressure level of the inlet liquid-borne noise decreases by 14 %, while the outlet decreases by 1 %, so the inlet liquid-borne noise measuring point is better for cavitation prediction. The inlet pressure pulsation intensity shows a decreasing trend, while the outlet is the opposite. The rate of change of inlet pressure pulsation intensity is more pronounced than the outlet. When the head drops by 3 %, the inlet pulsation intensity decreases by 66.3 %, while the outlet pulsation intensity increases by 13.9 %. The main frequency of the pressure pulsation signal is mainly distributed at the total blade passing frequency f_{BPF} . However, with the development of cavitation, the main frequency is influenced by the harmonic frequency, and some of the main frequencies are shifted. In summary, the inlet flange and pump casing axial vibration measuring points, inlet liquid-borne noise, and pressure pulsation measuring points have superior sensitivity and are suitable for cavitation fault diagnosis.

The arrangement of measuring points for cavitation fault diagnosis proposed in this work can be effectively applied to other pumps. The proposed method can be extended to the diagnosis of other pump faults, such as impeller damage, shaft misalignment, and shaft imbalance. However, regarding the thresholds for fault signal prediction, since different types of pumps have different performances and requirements, it is necessary to make specific judgments according to the actual situation. It can be further investigated in subsequent studies to improve the accuracy of cavitation fault diagnosis.

5 ACKNOWLEDGEMENTS

The authors would like to thank the financial support from National Natural Science Foundation of China (No. 51879122, 51779106), National Key Research and Development Program of China (Grant No. 2016YFB0200901, 2017YFC0804107), Zhenjiang key research and development plan (GY2017001, GY2018025), the Open Research Subject of Key Laboratory of Fluid and Power Machinery, Ministry of Education, Xi-hua University (szjj2017094, szjj2016068), Sichuan Provincial Key Lab of Process Equipment and Control (GK201614, GK201816), Jiangsu University Young Talent training Program-Outstanding Young backbone Teacher, Program Development of Jiangsu Higher Education Institutions (PAPD), and Jiangsu top six talent summit project (GDZB-017).

6 REFERENCES

- [1] Guan, X.F. (1995). *Handbook of Modern Pump Technology*, Astronautic Press, China.
- [2] Guo, X., Zhu, L., Zhu, Z., Cui, B., Li, Y. (2015). Numerical and experimental investigations on the cavitation characteristics of a high-speed centrifugal pump with a splitter-blade inducer. *Journal of Mechanical Science and Technology*, vol. 29, p. 259-267, DOI:10.1007/s12206-014-1232-x.
- [3] Luo, X.W., Ji, B., Tsujimoto, Y. (2016). A review of cavitation in hydraulic machinery. *Journal of Hydrodynamics*, vol. 28, p. 335-358, DOI:10.1016/S1001-6058(16)60638-8.
- [4] Dong, L., Shang, H., Zhao, Y., Liu, H., Wang, Y. (2019). Study on unstable characteristics of centrifugal pump under different cavitation stages. *Journal of Thermal Science*, vol. 28, p. 608-620, DOI:10.1007/s11630-019-1136-2.
- [5] Al-Obaidi, A.R. (2019). Effects of different turbulence models on three-dimensional unsteady cavitating flows in the centrifugal pump and performance prediction. *International Journal of Nonlinear Sciences and Numerical Simulation*, vol. 20, no. 3-4, p. 487-509, DOI:10.1515/ijnsns-2018-0336.
- [6] ISO 3555 (1977). *Centrifugal, Mixed Flow and Axial Pumps-Code for Acceptance Tests-Class B*. International Organization for Standardization, Geneva.
- [7] Stopa, M.M., Cardoso Filho, B.J., Martinez, C.B. (2013). Incipient detection of cavitation phenomenon in centrifugal pumps. *IEEE Transactions on Industry Applications*, vol. 50, no. 1, p. 120-126, DOI:10.1109/TIA.2013.2267709.
- [8] Harihara, P.P., Parlos, A.G. (2006). Sensorless detection of cavitation in centrifugal pumps. *ASME International Mechanical Engineering Congress and Exposition*, p. 187-192, DOI:10.1115/IMECE2006-14655.
- [9] Al-Hashmi, S., Gu, F., Li, Y., Ball, A. D., Fen, T., Lui, K. (2004). Cavitation detection of a centrifugal pump using instantaneous angular speed. *Engineering Systems Design and Analysis*, p. 185-190, DOI:10.1115/ESDA2004-58255.

- [10] Čudina, M., Prezelj, J. (2009). Detection of cavitation in situ operation of kinetic pumps: effect of cavitation on the characteristic discrete frequency component. *Applied Acoustics*, vol. 70, no. 9, p. 1175-1182, DOI:10.1016/j.apacoust.2009.04.001.
- [11] Čudina, M. (2003). Noise as an indicator of cavitation in a centrifugal pump. *Acoustical Physics*, vol. 49, no. 4, p. 463-474, DOI:10.1134/1.1591303.
- [12] Čudina, M. (2003). Detection of cavitation phenomenon in a centrifugal pump using audible sound. *Mechanical Systems and Signal Processing*, vol. 17, no. 6, p. 1335-1347, DOI:10.1006/mssp.2002.1514.
- [13] Černetič, J. (2009). The use of noise and vibration signals for detecting cavitation in kinetic pumps. *Proceedings of the Institution of Mechanical Engineers, Part C: Journal of Mechanical Engineering Science*, vol. 223, no. 7, p. 1645-1655, DOI:10.1243/09544062JMES1404.
- [14] Černetič, J., Čudina, M. (2011). Estimating uncertainty of measurements for cavitation detection in a centrifugal pump. *Measurement*, vol. 44, no. 7, p. 1293-1299, DOI:10.1016/j.measurement.2011.03.023.
- [15] Chini, S.F., Rahimzadeh, H., Bahrami, M. (2005). Cavitation detection of a centrifugal pump using noise spectrum. *International Design Engineering Technical Conferences and Computers and Information in Engineering Conference*, p. 13-19, DOI:10.1115/DETC2005-84363.
- [16] Wang, Y., Liu, H., Yuan, S., Tan, M., Wang, K. (2012). Experimental testing on cavitation vibration and noise of centrifugal pumps under off-design conditions. *Transactions of the Chinese Society of Agricultural Engineering*, vol. 28, no. 2, p. 35-38, DOI:10.3969/j.issn.1002-6819.2012.02.007. (in Chinese)
- [17] Zhang, N., Yang, M., Gao, B., Li, Z. (2015). Vibration characteristics induced by cavitation in a centrifugal pump with slope volute. *Shock and Vibration*, vol. 2015, art. ID 294980, DOI:10.1155/2015/294980.
- [18] Dong, L., Zhao, Y., Dai, C. (2019). Detection of inception cavitation in centrifugal pump by fluid-borne noise diagnostic. *Shock and Vibration*, vol. 2019, art. ID 9641478, DOI:10.1155/2019/9641478.
- [19] Al-Obaidi, A. R. (2020). Experimental comparative investigations to evaluate cavitation conditions within a centrifugal pump based on vibration and acoustic analyses techniques. *Archives of Acoustics*, vol. 45, no. 3, p. 541-556, DOI:10.24425/aoa.2020.134070.
- [20] Al-Obaidi, A. R. (2019). Investigation of effect of pump rotational speed on performance and detection of cavitation within a centrifugal pump using vibration analysis. *Heliyon*, vol. 5, no. 6, art. ID e01910, DOI:10.1016/j.heliyon.2019.e01910.
- [21] Al-Obaidi, A.R. (2020). Detection of cavitation phenomenon within a centrifugal pump based on vibration analysis technique in both time and frequency domains. *Experimental Techniques*, vol. 44, p. 329-347, DOI:10.1007/s40799-020-00362-z.
- [22] Al-Obaidi, A.R., Mishra, R. (2020). Experimental investigation of the effect of air injection on performance and detection of cavitation in the centrifugal pump based on vibration technique. *Arabian Journal for Science and Engineering*, vol. 45, p. 5657-5671, DOI:10.1007/s13369-020-04509-3.
- [23] Mousmoulis, G., Karlsen-Davies, N., Aggidis, G., Anagnostopoulos, I., Papantonis, D. (2019). Experimental analysis of cavitation in a centrifugal pump using acoustic emission, vibration measurements and flow visualization. *European Journal of Mechanics-B/Fluids*, vol. 75, p. 300-311, DOI:10.1016/j.euromechflu.2018.10.015.
- [24] Pan, Z.Y., Yuan, S.Q. (2013). *Fundamentals of Cavitation in Pumps*, Jiangsu University Press, Jiangsu.
- [25] Dong, L., Zhao, Y.Q., Dai, C., Wang, Y. (2018). Research on cavitation acoustic characteristics of centrifugal pump based on fluid-acoustic field coupling method. *Advances in Mechanical Engineering*, vol. 10, no. 5, DOI:10.1177/1687814018773665.
- [26] Yu, H. (2016). *Vibration Noise Measurement and Analysis Technology of Ship*. China Light Industry Press, p. 4-11.
- [27] Du, G. (2012). *Acoustic Fundamentals*. Nanjing university Press, Nanjing, p. 127-128.
- [28] Alahmadi, Y., Nowakowski, A. (2016). Modified shear stress transport model with curvature correction for the prediction of swirling flow in a cyclone separator. *Chemical Engineering Science*, vol. 147, p. 150-165, DOI:10.1016/j.ces.2016.03.023.